frontiers in Earth Science

ORIGINAL RESEARCH
published: 04 September 2020
doi: 10.3389/feart.2020.554924

Spatial Distribution of Rn, CO_2, Hg, and H_2 Concentrations in Soil Gas Across a Thrust Fault in Xinjiang, China

Yang Xiang[1,2], Xiaolong Sun[1]†, Dongying Liu[1], Long Yan[3], Bo Wang[4] and Xiaoqi Gao[1]*

[1] National Institute of Natural Hazards, MEMC, Beijing, China, [2] College of Geoscience and Surveying Engineering, China University of Mining and Technology, Beijing, China, [3] Earthquake Agency of the Xinjiang Uygur Autonomous Region, Ürümqi, China, [4] China Earthquake Networks Center, Beijing, China

OPEN ACCESS

Edited by:
Antonella Peresan, Istituto Nazionale di Oceanografia e di Geofisica Sperimentale (OGS), Italy

Reviewed by:
Iren Adelina Moldovan, Institutul National de Cercetare si Dezvoltare pentru Fizica Pamantului, Romania
Alessandra Sciarra, Istituto Nazionale di Geofisica e Vulcanologia (INGV), Italy
Giovanni Martinelli, National Institute of Geophysics and Volcanology, Section of Palermo, Italy

***Correspondence:**
Xiaolong Sun
xlsun04@163.com

†ORCID:
Xiaolong Sun
orcid.org/0000-0003-0807-3784

Specialty section:
This article was submitted to Solid Earth Geophysics, a section of the journal Frontiers in Earth Science

Received: *23 April 2020*
Accepted: *14 August 2020*
Published: *04 September 2020*

Citation:
Xiang Y, Sun X, Liu D, Yan L, Wang B and Gao X (2020) Spatial Distribution of Rn, CO_2, Hg, and H_2 Concentrations in Soil Gas Across a Thrust Fault in Xinjiang, China. Front. Earth Sci. 8:554924. doi: 10.3389/feart.2020.554924

Spatial distribution characteristics and origin of soil gasses were discussed in this study. We also examine the correlation between the spatial variation of soil gasses and fault activity, based on the measurements of Rn, Hg, H_2, and CO_2 concentrations in the eastern segment of the BLT fault zone in the southern Tianshan Mountains, Xinjiang, China. The results show that the Rn and CO_2 concentrations on the hanging wall were higher than those near the fault zone and on the footwall of the fault. Moreover, the Hg and H_2 concentrations on the footwall were also higher than those near the fault and on the hanging wall of the fault. The main factors affecting the variations in soil gas spatial distribution were gaseous origin structure of the crust, fault activity, fault fracture degree, stratigraphic lithology, and the cover layer. The results of active structural fault mapping show that the BLT fault has been active since the Late Quaternary and the thrust has broken the fault surface. Under the influence of tectonic compressive stress, the tension zone was formed on the hanging wall of the fault and fractures were developed. This result is consistent with the characteristics of soil gas concentrations measured in this study, indicating that the concentrations of Rn, Hg, H_2, and CO_2 are closely related to the fault activity. These findings can be applied to identify seismic precursors from gas monitoring data of the studied area.

Keywords: BLT fault, soil gas, spatial distribution, thrust fault, Xinjiang

INTRODUCTION

A fault zone is a channel for deflation of the crust, and the number of micro-cracks distributed in the fault zone randomly increases under the impact of the tectonic stress field. This accelerates the migration and release of deep gasses (Baubron et al., 2002; Pulinets and Dunajecka, 2007; Fu et al., 2017), and changes the concentration of chemical components near the fault (Wiersberg and Erzinger, 2008). General overviews of the geochemical, structural, and seismic features in tectonically active areas have shown some evidence of a correlation between soil gas geochemistry anomalies and tectonic activities. Evidence also shows that soil gas escaping through the fault and fractures in the active fault zones can be enhanced by fault and earthquake activity (Fu et al., 2008; Sciarra et al., 2017; Yuce et al., 2017). As such, analyzing the geochemical variations of soil gas near

fault zones has become an important method for investigating earthquake precursors, forecasting earthquakes, and evaluating fault activity (Li et al., 2013; Iovine et al., 2017).

Useful soil gasses include noble gasses, Rn, Hg, H_2, CO_2, and He, which play important roles in fault delineation and earthquake precursory studies (Chyi et al., 2005; Etiope et al., 2007; Caracausi and Paternoster, 2015; Camarda et al., 2016; Fu et al., 2017). Rn has been used by the scientific community as a tracer of natural phenomena related to outgassing from soil located along faults, fractures, and crustal discontinuities (King et al., 1996; Mazur et al., 1999). Rn concentration changes in soil gas and groundwater are commonly observed prior to earthquakes and volcanic eruptions; consequently, they have attracted considerable attention in studies of precursory geochemical signals (Morawska and Phillips, 1993; King et al., 1995; Giammanco et al., 2009; Walia et al., 2009; Iovine et al., 2017). Hg, H_2, He, CO_2, and CH_4 have also been utilized in revealing the relationship among fluid activities in fault zones (Ware et al., 1984; Sugisaki et al., 1996; Jones et al., 2010; Moore and Castro, 2012). Helium isotopes are of particular interest as they can provide unequivocal evidence for the presence in the crust of mantle-derived fluids; ^{3}He is essentially primordial and retained in the Earth's interior, whereas ^{4}He is mainly produced in the crust by the decay of U and Th. Hence, any ^{3}He/^{4}He ratio at the Earth's surface larger than the local and crustal production rates indicates the presence of mantle helium (Sano et al., 2016; Buttitta et al., 2020).

Active faults commonly exhibit anomalously high concentrations of various terrestrially generated gasses in groundwater and soil air (King, 1980, 1986; Sun et al., 2017b). Concentration abnormalities of soil gas were observed in the Tashkent earthquake area in Uzbek, San Andreas Fault in the United States, Hsinhua and Chaochou faults in southern Taiwan, and Longmenshan fault, Beichuan-Yingxiu fault, and Minjiang fault in China (Engle et al., 2001; Li et al., 2006; Fu et al., 2008; Walia et al., 2009; Zhou et al., 2010, 2015). These studies indicate that the application of soil gas concentrations near the fault zone is of great practical significance for studying the fault activity and capturing the precursory information of earthquakes.

In this study, the concentrations of Rn, Hg, H_2, and CO_2 in soil gas were measured in the field along the profiles approximately perpendicular to the BLT fault. The spatial distribution in the soil gas concentrations in the eastern segment of the BLT fault was analyzed. The BLT fault is a long-term successional active fault zone and has been active since the Late Quaternary. It controls the distribution of the Mesozoic and Cenozoic strata in the northern Tarim Basin (Yao et al., 2018). This study is the first to analyze the distribution characteristics of soil gas in the BLT fault.

OVERVIEW OF GEOLOGY AND SEISMOLOGY

The BLT fault is the boundary between the Tarim Basin and the South Tianshan, oriented along the NWW–EW direction. The length of the fault is approximately 300 km, and the fault plane is N-dipping with an inclination of 50–80° (**Figure 1**). The BLT fault cuts the Late Pleistocene and Holocene alluvial fans and has been active since the Late Quaternary. It forms clear large-scale paleoseismic deformation zones and fault scarps with different heights on the surface. According to the records, only M5.6 earthquakes in 1972 and M5.2 earthquakes in 1988 occurred along the BLT fault, and no large destructive earthquake has ever occurred. In the present study, we examine the Tiemenguan section of the eastern part of the BLT fault (hereinafter referred to as Tiemenguan). As shown in **Table 1**, since 1970, 12 earthquakes have occurred near the Tiemenguan section, including two earthquakes above M5 and M4 earthquakes. No earthquakes occurred during the study period, Only two earthquakes occurred after 2015, *M*4.6 on April 1, 2018, and *M*4.4 on May 9, 2020 (**Figure 1A**). However, these two earthquakes did not occur on the BLT fault. There are multiple terraces where the fault is faulted and the height of fault scarps varies between 2 and 20 m. According to the results of trench profile images, there have been more than two paleoseismic events in the fault segment since the late Pleistocene. The vertical displacement of the stratum caused by the latest paleoseismic event is 1.1 m (Yao et al., 2018). The surface strata near the fault are bent and flexed, forming a large number of bending faults, and the crustal shortening rate of SN is 1.43–1.81 mm/a. Large-scale earthquakes have not occurred in the BLT fault since the earliest recorded history. This indicates the potential for a large-scale earthquake to occur in the future. At the fault, the surface accumulation material is mainly gravel, primarily composed of granite, and also comprises limestone. The fault is exposed on the surface, and the overburden is mostly composed of fine sand or sandy sedimentary layers.

MEASUREMENT AND ANALYSIS METHODS

Figure 2 shows the schematic diagram for measuring Rn, Hg, CO_2, and H_2 concentrations. Before sampling, 0.8 m deep and 0.03 m wide holes were drilled in the soil at each sampling site. A pyramidal gas sampler was inserted into the hole after removing the drill bit. Before each measurement, the foreign gas in the samplers and in the rubber tube connecting the samplers and detector was removed prior to signal counting. The concentration of Rn in the soil gas was measured using AlphaGuard PQ 2000 PRO (AG) Radon Detector and the Hg concentrations were analyzed with portable RA-915+ Zeeman Mercury Analyzer. The error of measurement was 2 ng $\times$ m^{-3}. The concentration of CO_2 in the soil gas was measured using KG-3010E Portable Infrared CO_2 Analyzer, and the concentration of H_2 in the soil gas was measured by ATG-300H Portable Hydrogen Gauge with a detection limit of 0.01–10,000 ppm. In addition, five gas samples were collected following the drainage gas collection method at the fault zone for helium isotope (^{3}He/^{4}He) analysis. The container used for helium isotope detection was a 100 mL saline glass bottle. After the measurement of soil gas concentration, the gas in the sampler, connecting pipe, and air pump was removed using an air pump. The sampling container was cleaned with saturated saltwater three times, and then the gas was collected. The instrument used

TABLE 1 | Catalog of earthquakes occurring in the area near Tiemenguan from January 1, 1970 to May 31, 2020.

Date	Time (UTC)	Long (°E)	Lat (°N)	Mag (M)	Date	Time (UTC)	Long (°E)	Lat (°N)	Mag (M)
2020/5/9	12:11:19	85.640°	42.234°	4.4	1998/4/13	23:14:32	85.796°	41.995°	4
2018/4/1	1:18:36	85.580°	42.256°	4.6	1988/5/25	18:21:58	85.692°	42.010°	5.2
2014/9/9	12:04:57	85.196°	42.319°	4.4	1981/4/21	3:22:52	85.816°	41.988°	4.4
2013/8/28	12:57:41	85.776°	42.076°	4.5	1980/6/14	13:01:13	85.523°	41.954°	4.7
2013/7/9	14:51:55	85.276°	42.210°	4.3	1978/4/22	15:04:15	85.920°	42.004°	5.3
2005/6/3	19:11:23	85.770°	41.983°	4.1	1977/6/5	18:19:29	85.714°	42.004°	4.7

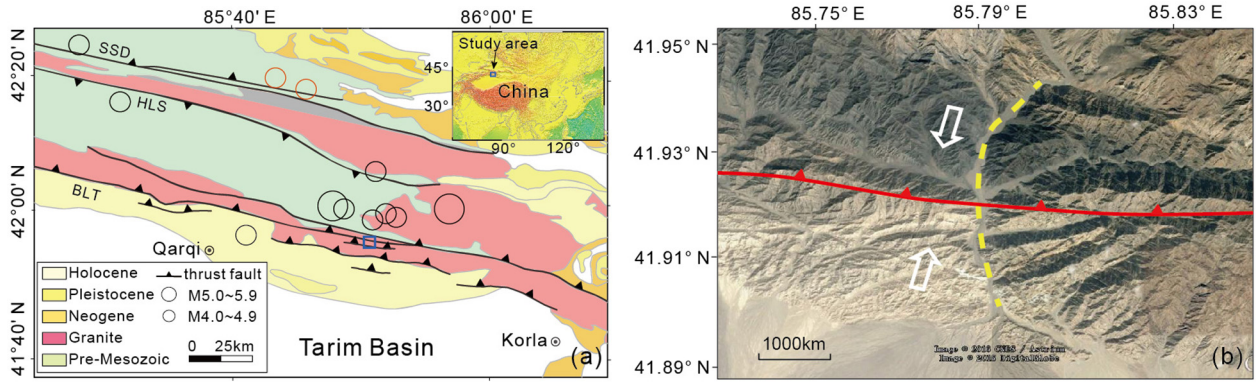

FIGURE 1 | Geologic structure map and seismic distribution of Tiemenguan section of BLT fault **(a)**, spatial distribution of soil gas survey lines **(b)**. The red circles indicate the earthquake that occurred after the measurement. SSD, Songshudaban fault; HLS, Huolashan fault; BLT, Beiluntai fault.

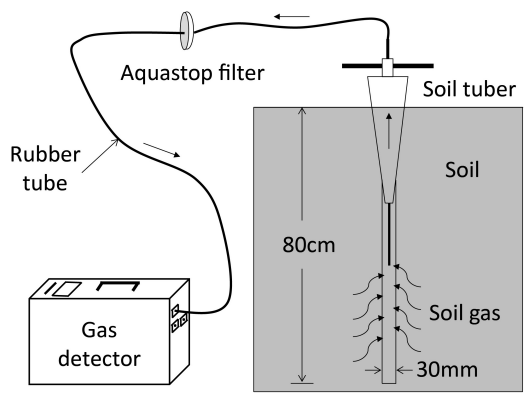

FIGURE 2 | Schematic diagram of soil gasses measurement.

was MM5400 mass spectrometer with a sensitivity greater than 1.5×10^{-6} a/PA. The gas samples were sent to the Lanzhou Center for Oil and Gas Resources Research, Institute of Geology and Geophysics, Chinese Academy of Sciences, immediately after the collection. Analysis of the samples was completed within 30 days of sampling.

Figure 3A shows that the measured values of Rn concentrations tended to stabilize after the second value of the initial measurement and there was a small amplitude of fluctuation. At each measurement time, 30 readings were taken and analyzed using the boxplot method, yielding a characteristic value of Rn concentration in each measurement site. The other three components, soil gas concentrations of CO_2, Hg, and H_2 were recorded based on the measurement time and their maximum values were taken. The concentration of soil gas CO_2 was relatively stable and the peaks were consistent with repeated measurements (**Figure 3B**). However, the concentrations of Hg and H_2 showed a gradual increase in the measured values and upon reaching the highest value, the concentrations tended to stabilize (**Figure 3C**) or rapidly decrease (**Figure 3D**).

RESULTS

In this study, soil gas measurements were obtained twice across the fault at Tiemenguan, the eastern segment of the BLT fault, Xinjiang. The results are shown in **Table 2**. During the first phase, the measurements of soil gas Rn and CO_2 concentrations were completed between April 20 and April 26, 2015. A total of 15 measuring points were identified from south to north. Measuring points 1–9 (P1–P9) were located at the footwall of the fault, and points 10 –15 (P10–P15) were located at the hanging wall of the fault. To determine whether there were similar changes in other gasses, we selected more measurement points at hanging wall (P13, P14, and P15), fault zone (P7, P8, and P10), and footwall (P2, P3, and P4) during the first phase from August 11–17, 2015, to conduct the second phase of soil gas measurements. The primary measurements recorded were the concentrations of Hg and H_2 in soil gas. As shown in **Figure 4**, due to the characteristics of H_2 (active) and Hg (adsorptive), such as the gas diffusion concentration that changes with time,

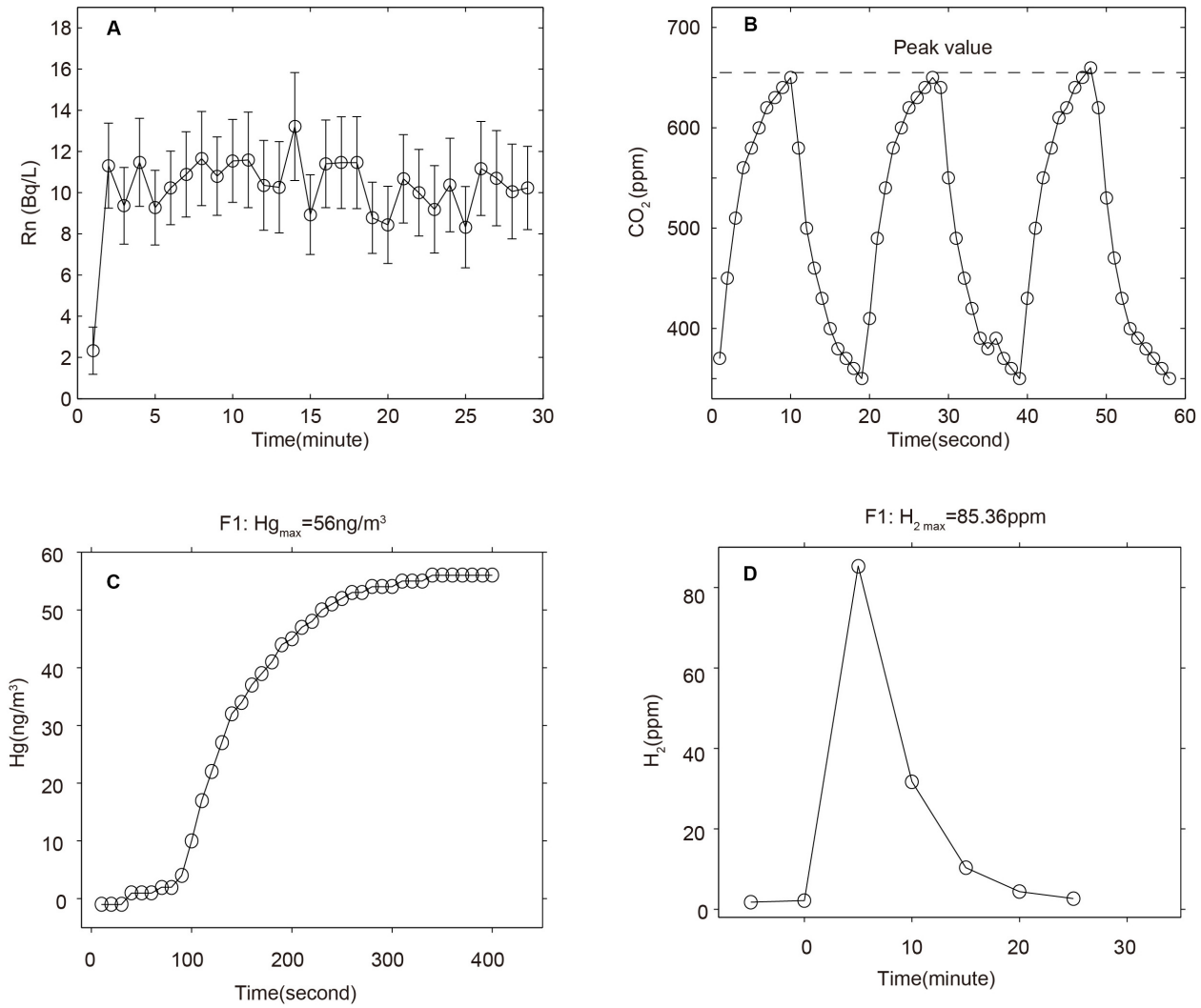

FIGURE 3 | The measurement curve of soil gas concentration in different components. The Rn concentration was determined according to the boxplot method to obtain the characteristics of Rn concentration at each site. A total of 30 measurements were acquired for each measurement point **(A)**. The other three components, soil gas concentration of CO_2, Hg and H_2 were recorded based on the measurement time, respectively. The peak of CO_2 concentration was the same after repeated measurements **(B)**, The Hg concentration value showed a steady change after rising to the highest value **(C)**, H_2 concentration characteristics showed a rapid decrease after rising to the highest value **(D)**. Therefore, the maximum value of the gas concentration curve of each component at sampling sites is analyzed.

the concentration of H_2 rapidly increased to the highest value and then decreased, while the concentration of Hg gradually increased to the highest value and then tended to stabilize. The maximum values of Hg and H_2 concentrations at each measuring point were obtained and the various characteristics of soil gas concentrations were analyzed.

As shown in **Figure 5E**, the terrain of the hanging wall of the fault is uplifted and that of the footwall is gentle. The survey line is vertical to the fault and extends approximately 2.5–3 km on both sides, with a total length of approximately 6 km. In addition, it should be noted that the study area is arid (i.e., precipitation and vegetation are not developed), with minimal soil moisture and stable temperature throughout the year, and the seasonal influence on soil gas concentrations is minimum in April and August.

The results show that in the footwall of the fault, the measured value of soil gas Rn concentration decreases toward the fault. It reaches the lowest value at the fault. However, in the hanging wall of the fault, the measured value increases toward the fault (**Figure 5A**). As shown in **Figure 5B**, the measured values of soil gas CO_2 concentration in the footwall of the fault (measuring points 1–9) are generally low, and the measured values decrease toward the exterior of the fault (measuring points 11 to 15). The concentrations of Rn and CO_2 are similar, and the measured values near the fault are high. The measured values gradually decrease with distance from the fault, and the concentration

TABLE 2 | Main statistic parameters of soil gas data in study area.

NO	Rn (Bq/L)	CO_2 (ppm)	Hg (ng/L)	H_2 (ppm)	$^3He/^4He$ R
P1	18.1686	520	–	–	–
P2	12.3266	910	59	85.36	–
P3	4.967	530	50	126.16	–
P4	10.1898	460	25	63.29	–
P5	4.1443	450	–	–	–
P6	2.3079	660	–	–	1.30×10^{-6}
P7	2.9054	470	10	37.04	1.21×10^{-6}
P8	7.6898	610	8	45.76	1.21×10^{-6}
P9	3.4503	480	–	–	1.38×10^{-6}
P10	17.6658	1510	7	48.64	1.23×10^{-6}
P11	13.6639	2110	–	–	–
P12	12.2356	1120	–	–	–
P13	8.2745	870	19	35.28	–
P14	8.2222	720	23	22.8	–
P15	6.883	360	16	47.84	–

measured in the hanging wall of the fault is higher than that in the footwall of the fault.

The Hg concentration of soil gas was the lowest near the fault (P7, P8, and P10) and was relatively high in the two walls of the fault. The concentrations in the footwall (P2–P4) were approximately twice as high as that in the hanging wall (P13–P15) (**Figure 5C**). The H_2 concentration of soil gas was higher in the footwall (P2–P4) and lower near the fault (P7, P8, and P10) and hanging wall (P13–P15) (**Figure 5D**).

In addition, helium isotope test results showed that the $^3He/^4He$ ratio ranges from 1.21×10^{-6} to 1.38×10^{-6}, which is lower than that of air (1.4×10^{-6}).

DISCUSSION

The measurement results show that the soil gas concentrations (Rn, CO_2, Hg, and H_2) in the Tiemenguan section in the BLT fault are different on either side of the fault zone. This may be closely related to the physical and chemical characteristics of the gas and its migration mechanism, the geological conditions of the measurement area, and the fracture development degree of the fracture zone.

Effect of Extent of Fracture Development on Soil Gas Concentration

The differences in soil gas concentrations are closely related to the distribution of fractures. The BLT fault is a thrust fault that is affected by the compressive force caused by regional tectonics. As shown in **Figure 1**, the bedrock type of BLT fault in the Tiemenguan section is primarily granite. Under regional tectonic compressive stress, a series of bending moment faults were formed in the hanging wall of the fault. Due to differences in the degrees of deformation in the hanging wall and footwall, their fractures exhibit different development degrees (**Figure 6**). As a result, the amount of deep gas escaping is different. In the hanging wall of the fault, under the regional tension stress environment, the surface at the top of the fault broke and formed a series of bending moment faults with many cracks. These bending moment faults are generally shallow fractures, allowing the gas in the soil to continuously escape to the atmosphere, which is not conducive to the enrichment of soil gas. On the other hand, the footwall topography, which is affected by compressive forces, is quite flat. The surface fractures are mainly closed or semi-closed, which is not suitable for the upward soil gas diffusion from the deep layers and its subsequent emission into the atmosphere. Thus, it is advantageous for the soil gas to be adsorbed on the particle surface of the rock. Then, it gradually accumulates in the soil. In the fault zone, the rock is highly fractured, and the fractures are further developed, which results in upward movement of the gas along the fracture.

Effect of Geological Conditions on Soil Gas Concentration

The spatial variation characteristics of soil gas concentration are not only related to the number of fractures on the fault, but also to the rock types and overburden properties. For

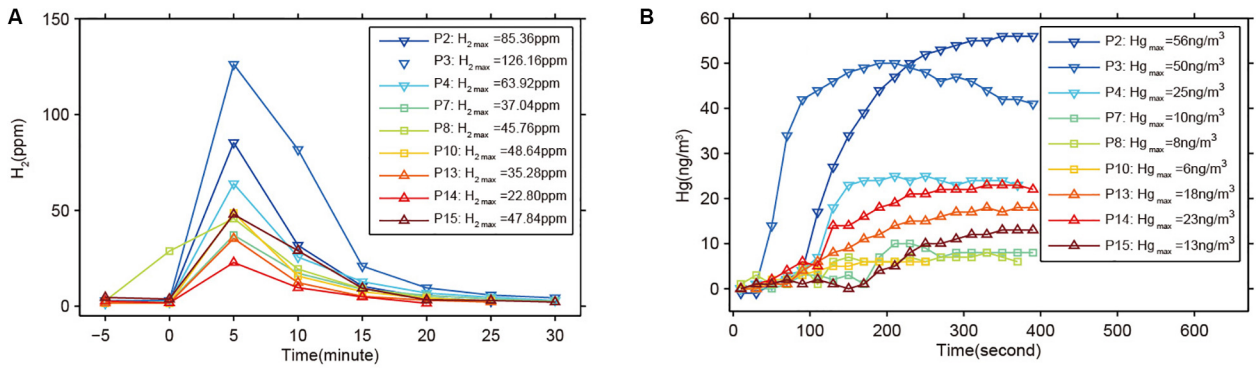

FIGURE 4 | Soil gas H_2 **(A)** and Hg **(B)** concentrations at nine sampling sites across the BLT fault zone at Tiemenguan. Different colors represent the variation cures of H_2 **(A)** and Hg **(B)** concentration of different measurement sites and the corresponding peaks.

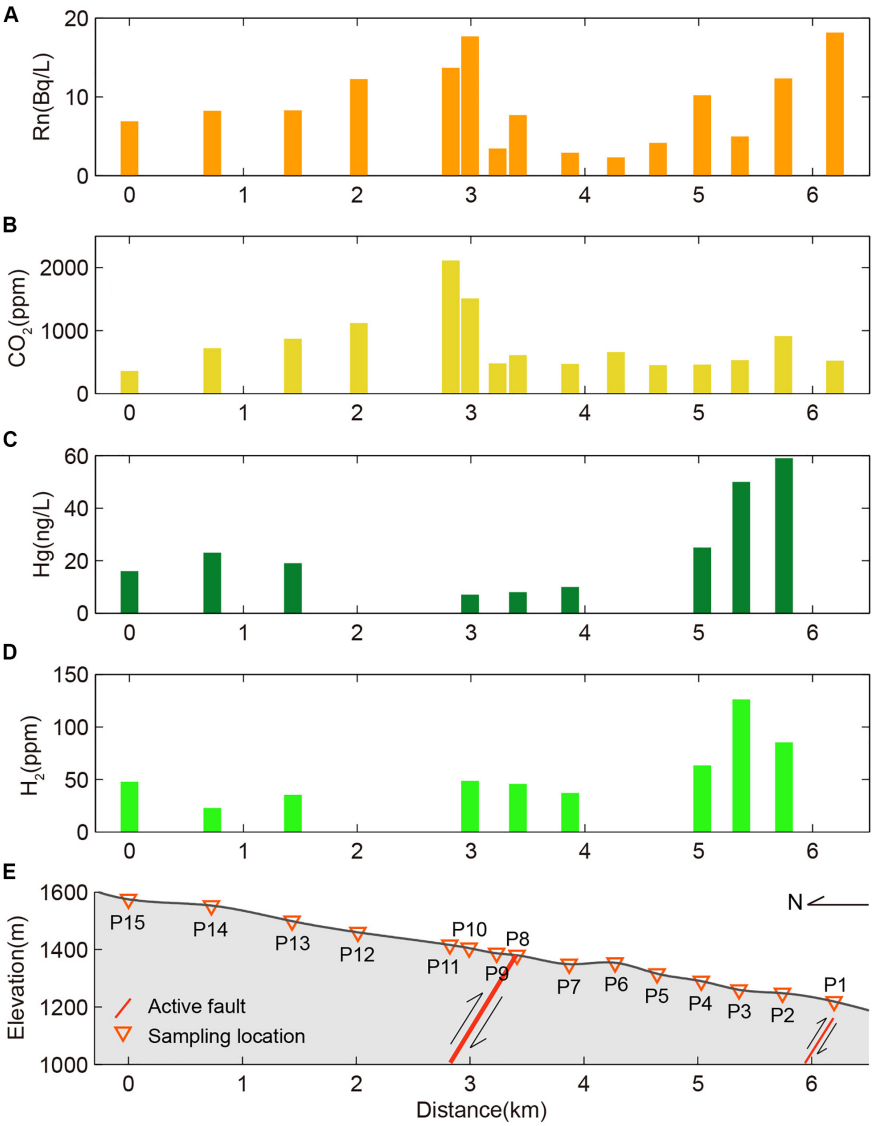

FIGURE 5 | Soil gas Concentrations of Rn **(A)**, CO_2 **(B)**, Hg **(C)**, and H2 **(D)** at Tiemenguan measuring point in BLT fault zone and distribution map of measuring points **(E)**. The north side is hanging wall, topographic uplift, south side is footwall, the terrain is gentle.

example, the surface sediments in the Tiemenguan section are primarily gravel and the rock types are mainly granite and limestone with high uranium and thorium content. This causes the soil gas Rn concentration in this section to be relatively high. Even if the rocks on either side of the fault are of the same type, different soil gas concentration characteristics will be formed if the overburden above the fault is different (Fu et al., 2005). As shown in **Figure 6**, there are differences in stratum type and overburden thickness between the two sides of the Tiemenguan fault. The hanging wall of the fault is covered with a thin layer of sandy soil; the fault is almost exposed to the surface, which results in the dilution of soil gas by air, and thus the soil gas concentration is low. The gravel layer in the footwall of the fault is comprised of weathered granite particles and medium coarse sand. The overburden layer is mainly sandy soil. It has strong gas sealing and adsorption properties. There are few channels available for the gas to escape and this results in a high gas concentration. This is reflected by the high concentrations of H_2 and Hg in the footwall of the fault.

Effects of Physical and Chemical Properties of Gasses

Hg is a heavy metal of great concern due to its extreme mobility and absorbability. Hg can be easily enriched in faults due to its special physical and chemical properties, and it can migrate from the interior to the surface along a fault or rock fracture due to fluid carrying or pressure gradient (Yangfen et al., 1989; Zhang et al., 2014; Sun et al., 2017a). H_2 is a relatively active

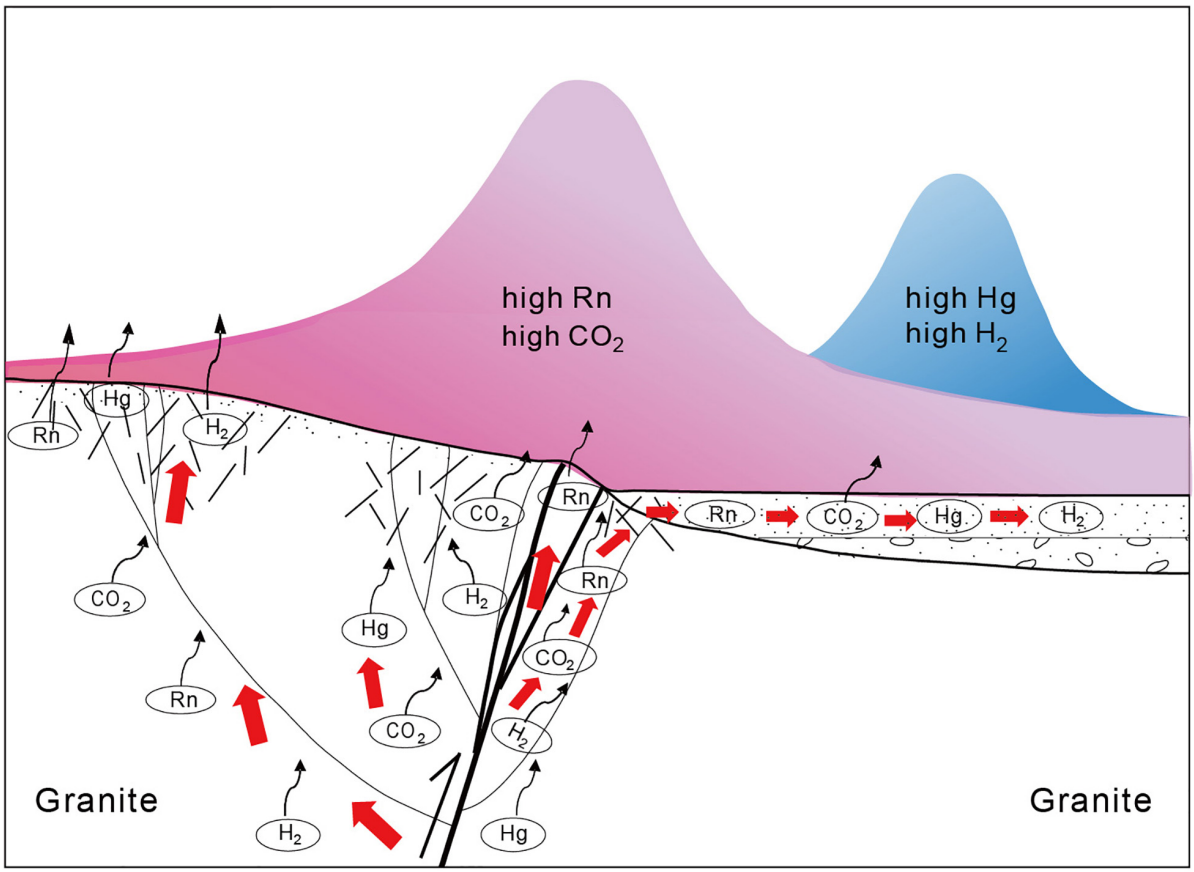

FIGURE 6 | Schematic diagram of thrust fault.

volatile substance and its diffusion speed is much higher than that of other gasses. It can easily migrate upward from the fault. The concentration of soil H_2 in the fault zone is closely related to the internal structure of the active fault and the development degree of fracture (Wakita et al., 1980). The sources of H_2 are as follows: microbial activity in shallow soil; deep water and abiogenic decomposition of CH_4 (King, 1986); and chemical reaction between fresh rock fracture surfaces and water (Sugisaki and Mizutani, 1983). CO_2 in the fault zone is usually a mixture of several source emissions. Surface biological activities or decomposition of organic matter may lead to increased CO_2 concentrations. However, active fault zones can directly produce a large amount of CO_2 and can also act as a channel to release deeply contained CO_2 (Ciotoli et al., 2007; Chiodini et al., 2008). Rn – a radioactive but chemically inert gas – is constantly generated all over the earth, normally in minute amount by radium in crustal materials (King et al., 1995). The short half-life of ^{222}Rn limits its diffusion in the soil; thus, the amount of radon measured at the ground surface cannot be released from a deep origin. Therefore, the concentration of Rn in soil gas is mainly affected by rocks containing radioactive elements U and Th. It also migrates from deep faults to the surface along with other carriers, such as CO_2, N_2, and CH_4 (Etiope and Martinelli, 2002; Yang et al., 2005; Chyi et al., 2010). The small carrier velocity can cause a large change in the concentration of the surface.

Changes in ^{3}He/^{4}He Isotope Ratio and Soil Gas Concentration

He is an inert gas with a small specific gravity and strong permeability. He in nature is mainly comes from the atmosphere, crust, and mantle. The helium in the atmosphere is mainly composed of ^{4}He, and the ^{3}He/^{4}He isotopic ratio is almost constant at 1.4×10^{-6}. The crust is dominated by radioactive atoms in rocks and minerals, such as radiogenic helium, with the ^{3}He/^{4}He value of 2.0×10^{-8} and the primary helium in the mantle, with the ^{3}He/^{4}He values ranging from 1.1×10^{-5} to 1.4×10^{-5}. R/Ra can represent the helium isotopic characteristics, where R is the ^{3}He/^{4}He ratio of the sample and Ra is the ^{3}He/^{4}He ratio of the atmosphere, i.e., 1.4×10^{-6}. When R/Ra <1, it represents the characteristic of shell source helium, while R/Ra > 1 represents the characteristic of mantle source helium. As shown in **Table 2**, the ^{3}He/^{4}He ratio of P6–P10 ranges from 1.21×10^{-6} to 1.38×10^{-6}. The calculation shows that R/Ra < 1 indicates that the helium in fault zone is formed from the crust; however, the ^{3}He/^{4}He ratio (1.21×10^{-6}–1.38×10^{-6}) at the fault zone is smaller than that in the

atmosphere (1.4×10^{-6}), which indicates that the helium from the crust has been diluted by atmospheric helium. The main causes of this effect are the U and Th contents in mineral rocks and the sealing characteristics of the system. The higher the content of U and Th in rocks, the more radioactive ^{4}He was that accumulated, and the sealing property of the system declined. The addition of helium outside the system changed the helium isotope ratio. The U and Th contents of the rocks are closely related to the Rn concentration, and the sealing property of the system is closely related to the ^{4}He. The addition of ^{4}He outside the system changes the helium isotope ratio. Therefore, the helium isotope results confirm the conjecture of this study.

Based on the above four aspects, we present the results of this paper. There may be two distinct reasons for the obvious difference in soil gas concentrations on either side of the fracture zone: one is the difference between the overburden layers and the other may be related to the fracture distribution in the fracture zone and its vicinity. As shown in **Figure 6**, the strain across the thrust faults is contractional. It causes the hanging wall to be highly deformed near the fault at the surface, resulting in local bending and extensional fractures that facilitate the upward escape of soil gas. It is not conducive to the enrichment of gas in shallow soil. Conversely, the surface fractures in the footwall are mostly closed, which is not suitable for the release of soil gas into the atmosphere, thus leading to the accumulation of gas in shallow soil. Therefore, the greater development of fractures in the hanging wall provides a good channel for gas escape, and the deep gas carriers, such as CO_2, can carry more Rn to the shallow surface and escape to the atmosphere. In the footwall, because there are fewer fractures, Rn in the deep soil layers cannot escape to the surface because of the short half-life period of 3.82 days and low migration rate; however, Hg and H_2 can reach the surface. Moreover, it is easy to enrich the surface of soil particles on the shallow surface with fewer fractures. In comparison, there are relatively high concentrations of Rn and CO_2 in the hanging wall (channel effect) and Hg and H_2 in the footwall (enrichment).

CONCLUSION

We obtained measurements of soil gas Rn, Hg, H_2, and CO_2 concentrations from the eastern section of the Beiluntai fault zone in the southern Tianshan Mountains, Xinjiang, China. The geochemical distribution characteristics of the soil gas along the eastern section of the Beiluntai fault were obtained and the possible reasons for the difference in concentrations of soil gas components in the fault were discussed. The following conclusions were drawn:

1. The concentration of the soil gas in the eastern segment of the Beiluntai fault zone in the southern Tianshan Mountains of Xinjiang showed a significant difference on either side of the fault. The concentration of Rn and CO_2 was higher on the hanging wall of the fault zone and the concentration of Hg and H_2 was higher on the footwall of the fault zone.
2. The soil gas Rn, Hg, H_2, and CO_2 concentrations of the fault zone are closely related to the physical and chemical characteristics, geological structure, and fracture distribution of the fault zone.

DATA AVAILABILITY STATEMENT

The raw data supporting the conclusions of this article will be made available by the authors, without undue reservation, to any qualified researcher.

AUTHOR CONTRIBUTIONS

YX and XS wrote the manuscript. All the authors participated in field measurements.

FUNDING

This research was supported by the research grants (ZDJ2019-06 and ZDJ2017-27) from National Institute of Natural Hazards, MEMC (former Institute of Crustal Dynamics, China Earthquake Administration) and National Natural Science Foundation of China (41972253).

REFERENCES

Baubron, J. C., Rigo, A., and Toutain, J. P. (2002). Soil gas profiles as a tool to characterise active tectonic areas: the Jaut Pass example (Pyrenees, France). *Earth Planet. Sci. Lett.* 196, 69–81. doi: 10.1016/s0012-821x(01)00596-9

Buttitta, D., Caracausi, A., Chiaraluce, L., Favara, R., and Sulli, A. (2020). Continental degassing of helium in an active tectonic setting (northern italy): the role of seismicity. *Sci. Rep.* 10:162.

Camarda, M., De Gregorio, S., Di Martino, R. M. R., and Favara, R. (2016). Temporal and spatial correlations between soil CO_2 flux and crustal stress. *J. Geophys. Res. Solid Earth* 121, 7071–7085. doi: 10.1002/2016jb013297

Caracausi, A., and Paternoster, M. (2015). Radiogenic helium degassing and rock fracturing: a case study of the southern Apennines active tectonic region. *J. Geophys. Res. Solid Earth* 120, 2200–2211. doi: 10.1002/2014jb011462

Chiodini, G., Caliro, S., Cardellini, C., Avino, R., Granieri, D., and Schmidt, A. (2008). Carbon isotopic composition of soil CO_2 efflux, a powerful method to discriminate different sources feeding soil CO_2 degassing in volcanic-hydrothermal areas. *Earth Planet. Scie. Lett.* 274, 372–379. doi: 10.1016/j.epsl.2008.07.051

Chyi, L. L., Quick, T. J., Yang, F. T., and Chen, C. H. (2005). Soil gas radon spectra and earthquakes. *Terrest., Atmosph. Oceanic Sci.* 16, 763–774. doi: 10.3319/TAO.2005.16.4.763(GIG)

Chyi, L. L., Quick, T. J., Yang, T. F., and Chen, C. H. (2010). The experimental investigation of soil gas radon migration mechanisms and its implication in earthquake forecast. *Geofluids* 10, 556–563. doi: 10.1111/j.1468-8123.2010.00308.x

Ciotoli, G., Lombardi, S., and Annunziatellis, A. (2007). Geostatistical analysis of soil gas data in a high seismic intermontane basin: fucino Plain central Italy. *J. Geophys. Res.* 112:B05407.

Engle, M. A., Gustin, M. S., and Zhang, H. (2001). Quantifying natural source mercury emissions from the Ivanhoe Mining District, north-central Nevada,USA. *Atmos. Environ.* 35, 3987–3997. doi: 10.1016/s1352-2310(01)00184-4

Etiope, G., and Martinelli, G. (2002). Migration of carrier and trace gases in the geosphere: an overview. *Phys. Earth Planet. Interiors* 129, 185–204. doi: 10.1016/s0031-9201(01)00292-8

Etiope, G., Martinelli, G., Caracausi, A., and Italiano, F. (2007). Methane seeps and mud volcanoes in Italy: gas origin, fractionation and emission to the atmosphere. *Geophys. Res. Lett.* 34:L14303.

Fu, C. C., Yang, T. F., Du, J., Walia, V., Chen, Y. G., Liu, T. K., et al. (2008). Variations of helium and radon concentrations in soil gases from an active fault zone in southern Taiwan. *Radiat. Measur.* 43, S348–S352.

Fu, C. C., Yang, T. F., Tsai, M. C., Lee, L. C., Liu, T. K., Walia, V., et al. (2017). Exploring the relationship between soil degassing and seismic activity by continuous radon monitoring in the Longitudinal Valley of eastern Taiwan. *Chem. Geol.* 469, 163–175. doi: 10.1016/j.chemgeo.2016.12.042

Fu, C. C., Yang, T. F., Walia, V., and Chen, C. H. (2005). Reconnaissance of soil gas composition over the buried fault and fracture zone in Southern Taiwan. *Geochem. J.* 39, 427–439. doi: 10.2343/geochemj.39.427

Giammanco, S., Immè, G., Mangano, G., Morelli, D., and Neri, M. (2009). Comparison between different methodologies for detecting radon in soil along an active fault: the case of the Pernicana fault system, Mt. Etna (Italy). *Appl. Radiat. Isot.* 67, 178–185. doi: 10.1016/j.apradiso.2008.09.007

Iovine, G., Guagliardi, I., Bruno, C., Greco, R., Tallarico, A., Falcone, G., et al. (2017). Soil-gas radon anomalies in three study areas of Central-Northern Calabria, (Southern Italy). *Nat. Hazards* 91, 193–219.

Jones, L. C., Rosenbauer, R., Goldsmith, J. I., and Oze, C. (2010). Carbonate control of H2 and CH4 production in serpentinization systems at elevated P-Ts. *Geophys. Res. Lett.* 37, 381–389.

King, C. Y. (1980). Episodic radon changes in subsurface soil gas along active faults and possible relation to earthquakes. *J. Geophys. Res. Solid Earth* 85, 3065–3078. doi: 10.1029/jb085ib06p03065

King, C. Y. (1986). Gas geochemistry applied to earthquake prediction: an overview. *J. Geophys. Res. Solid Earth* 91, 12269–12281. doi: 10.1029/jb091ib12p12269

King, C. Y., King, B. S., Evans, W. C., and Zhang, W. (1996). Spatial radon anomalies on active faults in California. *Appl. Geochem.* 11, 497–510. doi: 10.1016/0883-2927(96)00003-0

King, C. Y., Koizumi, N., and Kitagawa, Y. (1995). Hydrogeochemical anomalies and the 1995 Kobe earthquake. *Science* 269, 38–40. doi: 10.1126/science.269.5220.38

Li, Y., Du, J. G., Wang, X., Zhou, X. C., Xie, C., and Cui, Y. J. (2013). Spatial variations of soil gas geochemistry in the tangshan Area of Northern China. *Terrestr. Atmos. Ocean. Sci.* 24, 323–332. doi: 10.3319/tao.2012.11.26.01(tt)

Li, Y. G., Chen, P., Cochran, E. S., Vidale, J. E., and Burdette, T. (2006). Seismic evidence for rock damage and healing on the San Andreas Fault associated with the 2004 M6.0 *Parkfield earthquake*. *Bull. Seismol. Soc. Am.* 96, S349–S363.

Mazur, D., Janik, M., Łoskiewicz, J., Olko, P., and Swakoń, J. (1999). Measurements of radon concentration in soil gas by CR-39 detectors. *Radiat. Measur.* 31, 295–300. doi: 10.1016/s1350-4487(99)00135-3

Moore, C. W., and Castro, M. S. (2012). Investigation of factors affecting gaseous mercury concentrations in soils. *Sci. Total Environ.* 419, 136–143. doi: 10.1016/j.scitotenv.2011.12.068

Morawska, L., and Phillips, C. R. (1993). Dependence of the radon emanation coefficient on radium distribution and internal structure of the material. *Geochim. Cosmochim. Acta* 57, 1783–1797. doi: 10.1016/0016-7037(93)90113-b

Pulinets, S. A., and Dunajecka, M. A. (2007). Specific variations of air temperature and relative humidity around the time of Michoacan earthquake M8.1 Sept. 19,1985 as a possible indicator of interaction between tectonic plates. *Tectonophysics* 431, 221–230. doi: 10.1016/j.tecto.2006.05.044

Sano, Y., Takahata, N., Kagoshima, T., Shibata, T., Onoue, T., and Zhao, D. (2016). Groundwater helium anomaly reflects strain change during the 2016 Kumamoto earthquake in Southwest Japan. *Sci. Rep.* 6:37939.

Sciarra, A., Cantucci, B., and Coltorti, M. (2017). Learning from soil gas change and isotopic signatures during 2012 Emilia seismic sequence. *Sci. Rep.* 7:14187.

Sugisaki, R., Ito, T., Nagamine, K., and Kawabe, I. (1996). Gas geochemical changes at mineral springs associated with the 1995 southern Hyogo earthquake *(M* = 7.2) Japan. *Earth Planet. Sci. Lett.* 139, 239–249. doi: 10.1016/0012-821x(96)00007-6

Sugisaki, R., and Mizutani, Y. (1983). Origin of hydrogen and carbon dioxide in fault gases and its relation to fault activity. *J. Geol.* 91, 239–258. doi: 10.1086/628769

Sun, X., Si, X., Xiang, Y., and Liu, D. (2017a). Soil mercury spatial variations in the fault zone and corresponding influence factors. *Terrstr. Atmos. Ocean. Sci.* 28, 283–294. doi: 10.3319/tao.2016.09.29.02

Sun, X., Yang, P., Xiang, Y., Si, X., and Liu, D. (2017b). Across-fault distributions of radon concentrations in soil gas for different tectonic environments. *Geosci. J.* 22, 227–239. doi: 10.1007/s12303-017-0028-2

Wakita, H., Nakamura, Y., Kita, I., Fujii, N., and Notsu, K. (1980). Hydrogen release: new indicator of fault activity. *Science* 210, 188–190. doi: 10.1126/science.210.4466.188

Walia, V., Yang, T. F., Hong, W. L., Lin, S. J., Fu, C. C., Wen, K. L., et al. (2009). Geochemical variation of soil–gas composition for fault trace and earthquake precursory studies along the Hsincheng fault in NW Taiwan. *Appl. Radiat. Isot.* 67, 1855–1863. doi: 10.1016/j.apradiso.2009.07.004

Ware, R. H., Roecken, C., and Wyss, M. (1984). The detection and interpretation of hydrogen in fault gases. *Pure Appl. Geophys.* 122, 392–402. doi: 10.1007/bf00874607

Wiersberg, T., and Erzinger, J. (2008). Origin and spatial distribution of gas at seismogenic depths of the San Andreas fault from drill-mud gas analysis. *Appl. Geochem.* 23, 1675–1690. doi: 10.1016/j.apgeochem.2008.01.012

Yang, T. F., Walia, V., Chyi, L. L., Fu, C. C., Chen, C. H., Liu, T. K., et al. (2005). Variations of soil radon and thoron concentrations in a fault zone and prospective earthquakes in SW Taiwan. *Radiat. Measur.* 40, 496–502. doi: 10.1016/j.radmeas.2005.05.017

Yangfen, J., Zonghua, W., Chunsheng, S., Jiazhen, W., and Hongren, Z. (1989). Earthquake prediction through the observation and measurement of mercury content variation in water. *J. Geochem. Explorat.* 33, 195–202. doi: 10.1016/0375-6742(89)90029-0

Yao, Y., Song, H. P., Chen, J. B., Li, S., and Jia, H. L. (2018). Late quaternary crustal shortening rate of the Beiluntai fault in southern. *Seismol. Geol.* 40, 71–86.

Yuce, G., Fu, C. C., D'Alessandro, W., Gulbay, A. H., Lai, C. W., Bellomo, S., et al. (2017). Geochemical characteristics of soil radon and carbon dioxide within the Dead Sea fault and Karasu fault in the Amik basin, (Hatay), Turkey. *Chem. Geol.* 469, 129–146. doi: 10.1016/j.chemgeo.2017.01.003

Zhang, L., Liu, Y., Guo, L., Yang, D., Fang, Z., Chen, T., et al. (2014). Isotope geochemistry of mercury and its relation to earthquake in the Wenchuan Earthquake Fault Scientific drilling project hole-1. (WFSD-1). *Tectonophysics* 619–620, 79–85. doi: 10.1016/j.tecto.2013.08.025

Zhou, X., Wang, W., Chen, Z., Yi, L., Liu, L., Xie, C., et al. (2015). Hot spring gas geochemistry in western sichuan province, China after the wenchuan ms 8.0 earthquake. *Terr. Atmos. Ocean. Sci.* 26, 361–373. doi: 10.3319/tao.2015.01.05.01(tt)

Zhou, X. C., Du, J. G., Chen, Z., Cheng, J. W., Tang, Y., Yang, L. M., et al. (2010). Geochemistry of soil gas in the seismic fault zone produced by the Wenchuan Ms = 8.0 earthquake, southwestern China. *Geochem. Trans.* 11:5.

Conflict of Interest: The authors declare that the research was conducted in the absence of any commercial or financial relationships that could be construed as a potential conflict of interest.